Support Information

Extraordinary self-powered Y-shaped flexible film thermoelectric device for wearables

Xinjie Yuan[a,b], Pengfei Qiu*[a,b,c], Chuanyao Sun[a,b], Shiqi Yang[a], Yi Wu[a,b], Lidong Chen[a,b], Xun Shi*[a,b]

[a]State Key Laboratory of High Performance Ceramics and Superfine Microstructure, Shanghai Institute of Ceramics, Chinese Academy of Sciences, Shanghai 200050, China.

[b]Center of Materials Science and Optoelectronics Engineering, University of Chinese Academy of Sciences, Beijing 100049, China

[c]School of Chemistry and Materials Science, Hangzhou Institute for Advanced Study, University of Chinese Academy of Sciences, Hangzhou 310024, China

*Corresponding authors.

E-mails: qiupf@mail.sic.ac.cn, xshi@mail.sic.ac.cn.

This file contains:

- Figure S1 to S11
- Table S1 to S6
- References

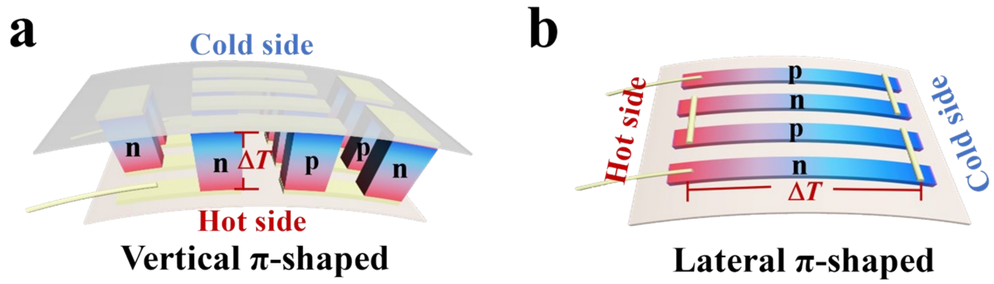

Figure S1. Schematics of flexible film TE devices. (a) vertical π-shaped configuration and (b) lateral π-shaped configuration.

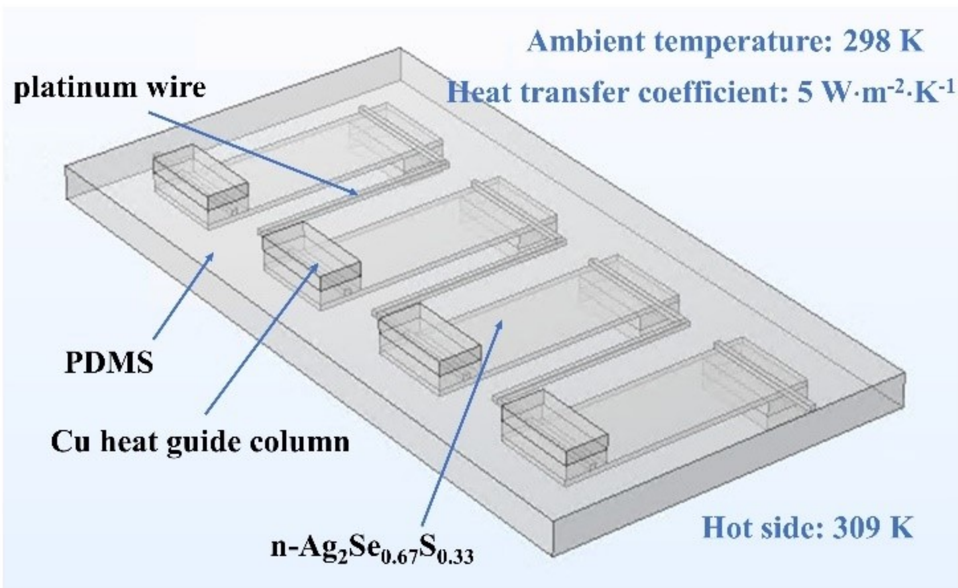

Figure S2. Schematics of the Y-shaped flexible film TE device used for the three-dimensional finite element simulation. It contains four $Ag_2Se_{0.67}S_{0.33}$ legs. Some boundary conditions are listed in the figure.

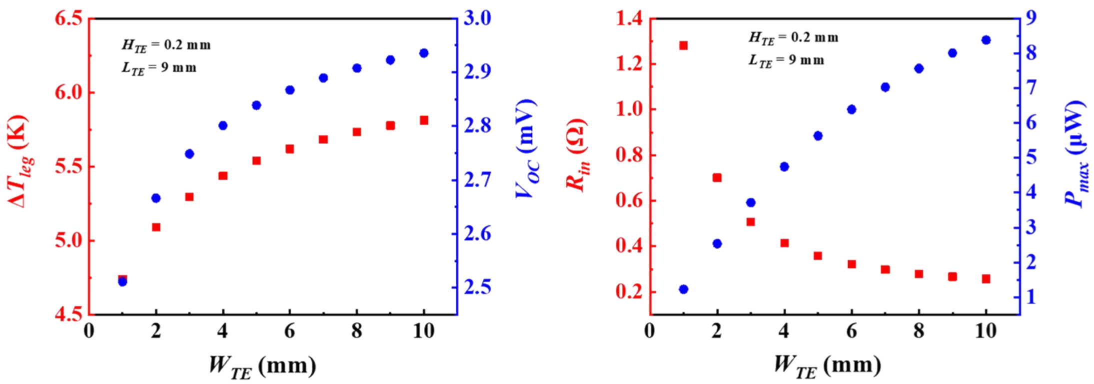

Figure S3. Simulated ΔT_{leg}, V_{max}, R_{in}, and P_{max} of a Y-shaped flexible film TE device including four $Ag_2Se_{0.67}S_{0.33}$ legs under different W_{TE}. In the simulation, H_{TE} is set as 0.2 mm and L_{TE} is set as 9 mm. The hot side temperature is set as 309 K and the ambient temperature is set as 298 K. The heat transfer coefficient is set as 10 $W \cdot m^{-2} \cdot K^{-1}$.

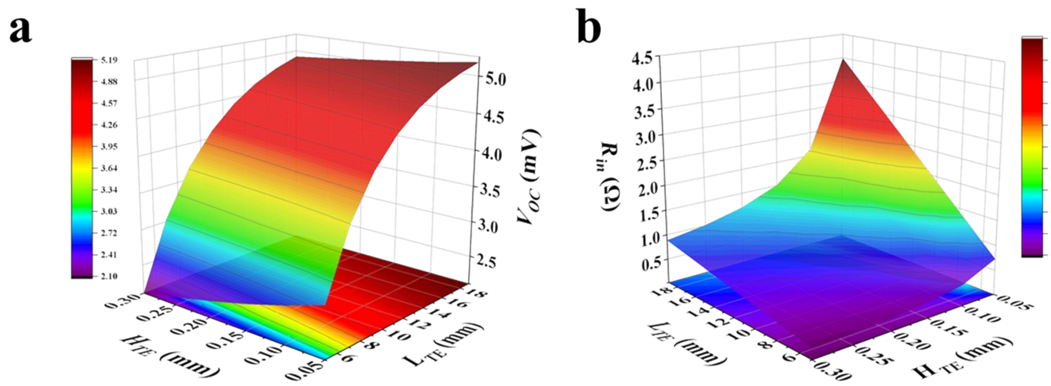

Figure S4. 3D finite element simulation of the device's performance. (a) Open-circuit voltage (V_{OC}) and (b) internal resistance (R_{in}) of a Y-shaped flexible film TE device containing four $Ag_2Se_{0.67}S_{0.33}$ legs under different height (H_{TE}) and length (L_{TE}). The model used for the simulation is shown in Figure S2. The heat transfer coefficient (h_{air}) is set as 10 $W \cdot m^{-2} \cdot K^{-1}$. The hot side temperature is set as 309 K and the ambient temperature is set as 298 K.

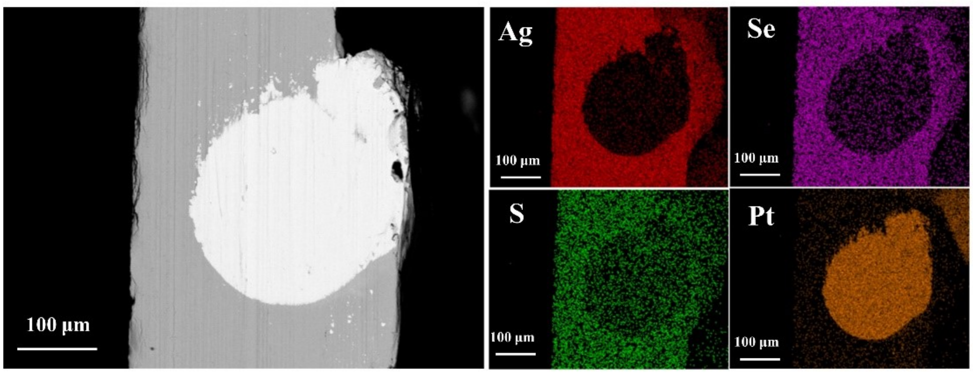

Figure S5. Backscattered electron image and elemental energy dispersive spectroscopy (EDS) mappings at the interface between $Ag_2Se_{0.67}S_{0.33}$ and platinum wire.

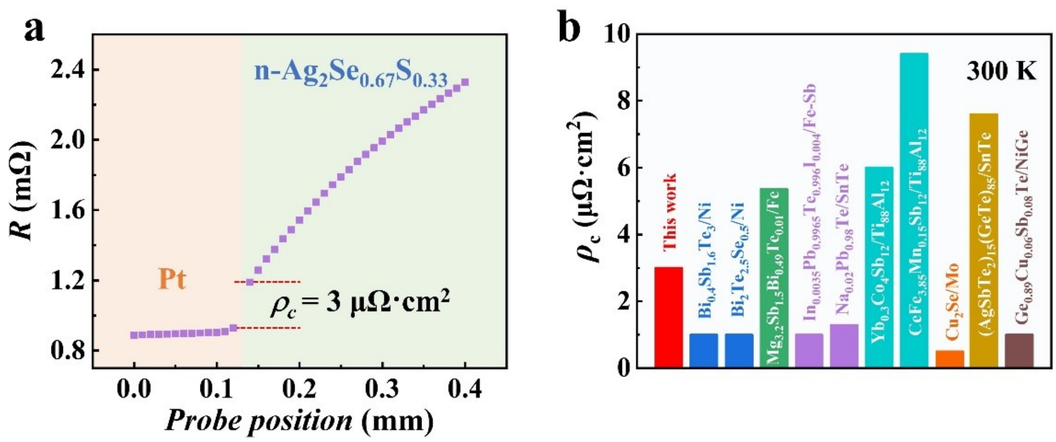

Figure S6. Contact electrical resistivity of $Ag_2Se_{0.67}S_{0.33}$/Pt interface. (a) Resistance (*R*) line scanning across the $Ag_2Se_{0.67}S_{0.33}$/Pt interface. (b) Comparison on the contact electrical resistivity (ρ_c) of typical TE materials and metals. The detailed data can be found in Table S2.

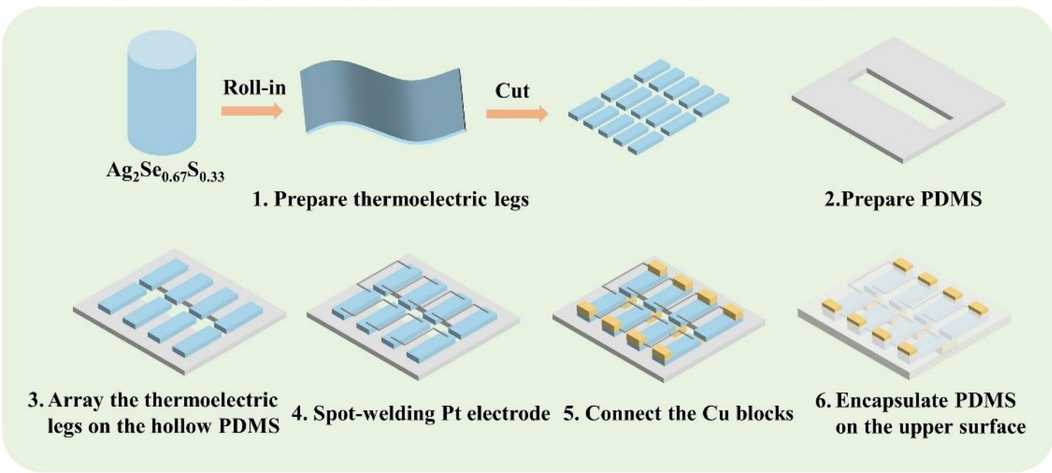

Figure S7. Schematics of the preparation process for the Y-shaped flexible film TE device.

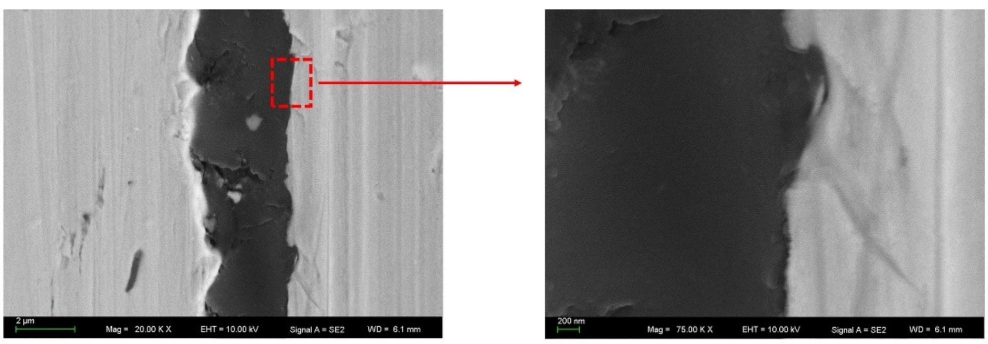

Figure S8. Scanning electron microscopy image of the interface between thermally conductive copper block and $Ag_2Se_{0.67}S_{0.33}$TE leg.

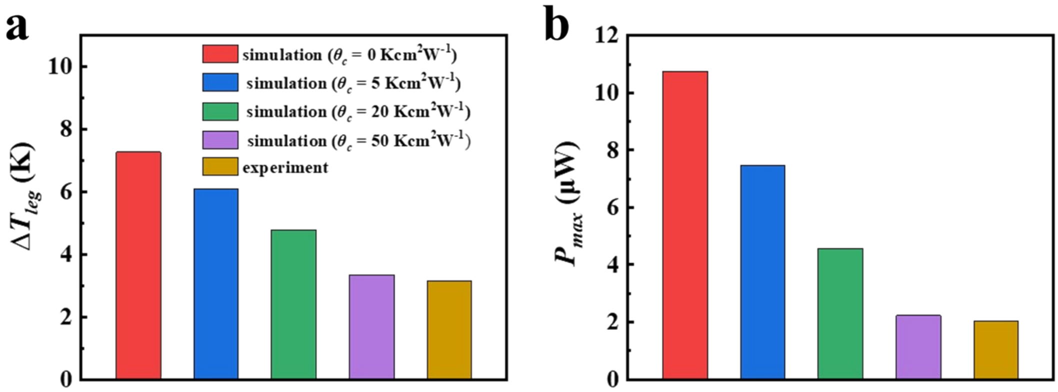

Figure S9. Simulated and measured (a) ΔT_{leg} and (b) P_{max} of a Y-shaped flexible film TE device including 4 $Ag_2Se_{0.67}S_{0.33}$ legs. The H_{TE} is set as 0.2 mm and the L_{TE} is set as 9 mm. In the simulation, the ambient temperature is set as 298 K and the hot side temperature is set as 309 K. The h_{air} is set as 10 W·m^{-2}·K^{-1}. The θ_c is set as 0 Kcm^{2}W^{-1}, 5 Kcm^{2}W^{-1}, 20 Kcm^{2}W^{-1}, and 50 Kcm^{2}W^{-1}, respectively. In the experiment, the ambient temperature is set as 298 K and the hot plate temperature is set as 309 K. The wind speed is set as 0 m·s^{-1}.

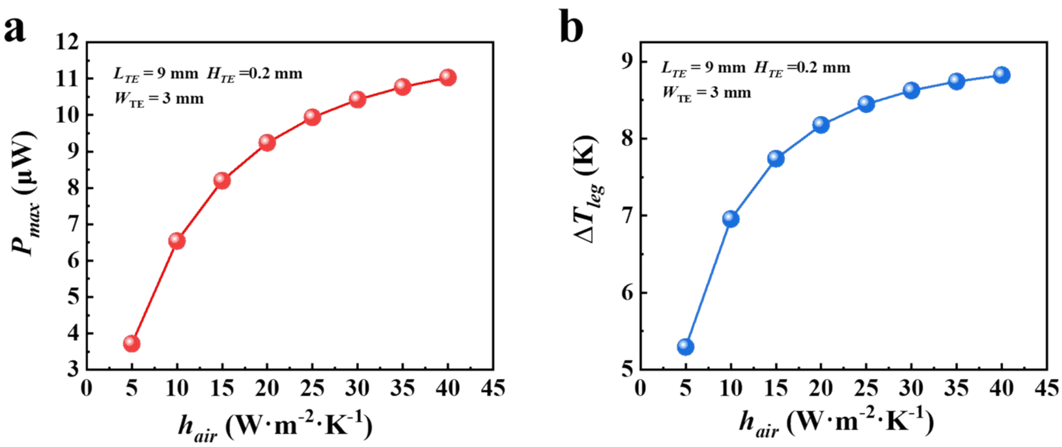

Figure S10. Simulated maximum output power (P_{max}) and temperature difference (ΔT_{leg}) for the Y-shaped flexible film TE device under different heat transfer coefficient (h_{air}). The length of the uni-leg (L_{TE}) is set as 9 mm, H_{TE} is set as 0.2 mm and W_{TE} is set as 3 mm. The hot side temperature is set as 309 K and the ambient temperature is set as 298 K.

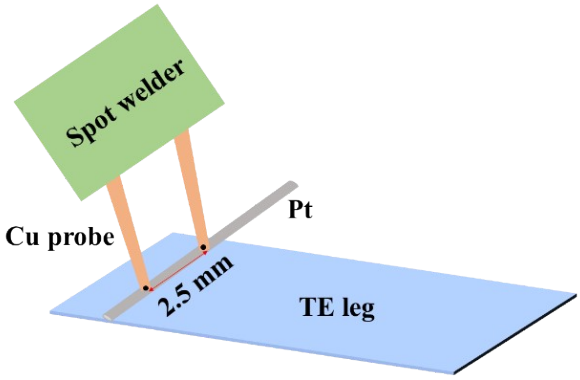

Figure S11. Schematics of the spot-welding method used in this work. The distance between the two Cu probes is about 2.5 mm.

Table S1. Comparison on the output performance of different kinds of flexible film TE devices. Power density (P_{max}/A, where P_{max} is the maximum power output and A is the cross-sectional area of the device) and corresponding open-circuit voltage (V_{OC}) of Y-shaped flexible film TE device developed in this work and typical flexible film TE devices reported before. All data are taken from the condition when the device is worn on human body.

	Composition	V_{OC} (mV)	P_{max}/A (μW·cm^{-2})	Reference
Y-shaped	n-$Ag_2Se_{0.67}S_{0.33}$	16.5 41.7 27	0.2 1.1 0.55	This work
	PEDOT:PSS/CNT/Bi_2Te_3	1.2	8.1×10^{-4}	1
Vertical π-shaped	n-$Ag_{20}S_7Te_3$ p-$(AgCu)_{0.998}Se_{0.22}S_{0.08}Te_{0.7}$	0.2	0.01	2
	n-Bi_2Te_3 p-Sb_2Te_3	2.9	0.72	3
Lateral π-shaped	n-SWCNT/PEI p-SWCNT/PAA	61.4	4.3×10^{-3}	4
	n-PEDOT:PSS p-SWCNT/P3HT	6.1	1.2×10^{-4}	5
	n-Bi_2Te_3 p-$Bi_{0.5}Sb_{1.5}Te_3$	4.1	1.1×10^{-4}	6
	p-EG_3-$GIC2_7$	3.7	1.8×10^{-4}	7
	n-Ag_2Se	3.1	1.8×10^{-2}	8
	n-$Ag_{1.8}Se$	3.5	2.6×10^{-4}	9
	n-Cu-doped Ag_2Se	2.1	2.7×10^{-4}	10
	n-WS_2 p-$NbSe_2$	2.4	6.7×10^{-4}	11

Table S2. Contact electrical resistivity (ρ_c) for typical TE materials.

	ρ_c (μΩ·cm^2)	Reference
$Ag_2S_{0.33}Se_{0.67}$/Pt	3	This work
$Bi_{0.4}Sb_{1.6}Te_3$/Ni	1	12
$Bi_2Te_{2.5}Se_{0.5}$/Ni	1	13
$Mg_{3.2}Sb_{1.5}Bi_{0.49}Te_{0.01}$/Fe	5.4	14
$In_{0.0035}Pb_{0.9965}Te_{0.996}I_{0.004}$/Fe-Sb	1	15
$Na_{0.02}Pb_{0.98}$Te/SnTe	1.3	15
$Yb_{0.3}Co_4Sb_{12}$/$Ti_{88}Al_{12}$	6	13
$CeFe_{3.85}Mn_{0.15}Sb_{12}$/$Ti_{88}Al_{12}$	9.4	13
$(AgSbTe_2)_{15}(GeTe)_{85}$/SnTe	7.6	16

Cu_2Se/Mo	0.5	[17]
$Ge_{0.89}Cu_{0.06}Sb_{0.08}Te/NiGe$	1	[18]

Table S3. Normal internal resistivity ($R_{in}S/Nl$, where N is the number of TE legs in the device, S and l are the cross-section area and length of one TE leg inside the device, respectively) of the flexible film TE device developed in this work and the traditional lateral π-shaped flexible film TE devices reported before.

	Composition	$R_{in}S/Nl$ (Ω·m)	Reference
Ag_2Se-based	Ag_2Se	5.7×10^{-5}	[8]
	n-$Ag_2Se/Ag/CuAgSe$	7×10^{-4}	[19]
	Ag_2Se	1.6×10^{-4}	[20]
	n-$Ag_{1.8}Se$	2.5×10^{-4}	[9]
	n-BC/Ag_2Se	1.7×10^{-3}	[21]
Bi_2Te_3-based	n-Bi_2Te_3 p- Sb_2Te_3	3.2×10^{-4}	[22]
	p-$Bi_{0.4}Sb_{1.6}Te_3$	3.4×10^{-5}	[23]
	n-$Bi_2Te_{2.7}Se_{0.3}$ p-$Bi_{0.5}Sb_{1.5}Te_3$	1.5×10^{-3}	[24]
	n- Bi_2Te_3/CFF	3.5×10^{-3}	[25]
	n-Bi_2Te_3 p-$Bi_{0.5}Sb_{1.5}Te_3$	2.6×10^{-4}	[6]
Organic-based	n-$C_{60}TiS_2$ p-PEDOT:PSS/SWCNTs	2.1×10^{-5}	[26]
	p-PANI/SWCNTs	2.2×10^{-5}	[27]
	p-PEDOT:PSS	1.1×10^{-4}	[28]
	p-PVDF/SWCNT	5.2×10^{-3}	[29]
	p-PEDOT:PSS	2.0×10^{-4}	[30]
	$Ag_2Se_{0.67}S_{0.33}$	1.1×10^{-5}	This work

Table S4. Temperature difference (ΔT_{leg}) built across the TE legs in the Y-shaped flexible film TE device prepared in this work and some vertical π-shaped flexible TE devices consisting of film and bulk TE legs reported before. All data are taken from the condition when the device is worn on human body.

	Composition	T_{air} (K)	ΔT_{leg} (K)	Reference
	n-$Ag_2Se_{0.67}S_{0.33}$	293	2.2	This work
		293	5.6	
		293	3.6	
Vertical	n-$Ag_{20}S_7Te_3$	298	0.1	[2]

π-shaped (film TE legs)	p-$(AgCu)_{0.998}Se_{0.22}S_{0.08}Te_{0.7}$			
	n-Bi_2Te_3 p-Sb_2Te_3	288	1.1	3
Vertical π-shaped (bulk TE legs)	n-$Bi_2Se_{0.3}Te_{2.7}$ p-$Bi_{0.4}Sb_{1.6}Te_3$	295	1.56	31
	n-$Bi_2Se_{0.3}Te_{2.7}$ p-$Bi_{0.5}Sb_{1.5}Te_3$	297	0.27	32
	n-$Bi_2Se_{0.3}Te_{2.7}$ p-$Bi_{0.5}Sb_{1.5}Te_3$	296	1.36	33
	n-$Bi_2Se_{0.3}Te_{2.7}$ p-$Bi_{0.5}Sb_{1.5}Te_3$	294	1.8	34
	n-$Bi_2Se_{0.3}Te_{2.7}$ p-$Bi_{0.5}Sb_{1.5}Te_3$	294	1.2	35
	n-$Bi_2Se_{0.3}Te_{2.7}$ p-$Bi_{0.5}Sb_{1.5}Te_3$	290	1.54	36

Table S5. Maximum power generated by per TE leg (P_{max}/N, where N is the number of TE legs in the device) for the Y-shaped flexible film TE device prepared in this work and reported before and some lateral π-shaped flexible film TE devices reported before.

	Composition	ΔT_{leg} (K)	P_{max}/N (μW)	Reference
Y-shaped	n-$Ag_2Se_{0.67}S_{0.33}$	2.5 5.7 3.6	0.11 0.59 0.29	This work
	n-Bi_2Te_3 p-Sb_2Te_3	7.3	6.3×10^{-2}	37
	PEDOT:PSS/CNT/Bi_2Te_3	3.9	3.3×10^{-3}	1
	n-Bi_2Te_3 p-$Bi_{0.3}Sb_{1.7}Te_3$	6.65	2.3×10^{-3}	38
Lateral π-shaped	n-SWCNT/PEI p-SWCNT/PAA	5.1	6.4×10^{-4}	4
	n-PEDOT:PSS p-SWCNT/P3HT	8	1.3×10^{-4}	5
	n-Bi_2Te_3 p-$Bi_{0.5}Sb_{1.5}Te_3$	7	3.4×10^{-5}	6
	p-EG_3-$GIC2_7$	3.9	6.4×10^{-4}	7
	n-Ag_2Se	2	1.8×10^{-2}	8
	n-$Ag_{1.8}Se$	5.8	5.8×10^{-4}	9
	n-Cu-doped Ag_2Se	1.8	7.4×10^{-4}	10

Table S6. Detailed material parameters used in the simulation.

	Electrical conductivity ($S·m^{-1}$)	**Thermal conductivity ($W·m^{-1} K^{-1}$)**	**Seebeck coefficient ($\mu V·K^{-1}$)**	**Density ($kg·m^{-3}$)**	**Heat capacity ($J·kg^{-1}·K^{-1}$)**
$Ag_2Se_{0.67}S_{0.33}$	1.2×10^5	1.1	-125	7986	267.53
Pt electrodes	8.9×10^6	71.6	\	21450	133
Copper	6×10^7	400	\	8960	385
PDMS	\	0.16	\	970	1460

References

1 D. Ding, Q. Wu, Q. Li, Y. Chen, C. Zhi, X. Wei and J. Wang, *Small*, 2023, **20**, 2306830.

2 Q. Yang, S. Yang, P. Qiu, L. Peng, T.-R. Wei, Z. Zhang, X. Shi, and L. Chen, *Science*, 2022, **377**, 854–858.

3 S. J. Kim, J. H. We and B. J. Cho, *Energy Environ. Sci.*, 2014, **7**, 1959–1965.

4 S. Hwang, D. Jang, B. Lee, Y.-S. Ryu, J. Kwak, H. Kim and S. Chung, *Adv. Energy Mater.*, 2023, **13**, 2204171.

5 S.-H. Hong, T.-C. Lee and C.-L. Liu, *ACS Appl. Energy Mater.*, 2023, **6**, 2602–2610.

6 Q. Zou, H. Shang, D. Huang, B. Xie, L. Zhang, K. Wang, H. Dong, C. Li, H. Gu and F. Ding, *Appl. Phys. Lett.*, 2022, **120**, 023903.

7 S. Sun, X.-L. Shi, W.-D. Liu, T. Wu, D. Wang, H. Wu, X. Zhang, Y. Wang, Q. Liu, and Z.-G. Chen, *ACS Appl. Mater. Interfaces*, 2022, **14**, 8066–8075.

8 Y. Liu, Y. Lu, Z. Wang, J. Li, P. Wei, W. Zhao, L. Chen and K. Cai, *J. Mater. Chem. A*, 2022, **10**, 25644–25651.

9 S. Hou, Y. Liu, L. Yin, C. Chen, Z. Wu, J. Wang, Y. Luo, W. Xue, X. Liu, Q. Zhang, and F. Cao, *Nano Energy*, 2021, **87**, 106223.

10 S. Hou, *Cell Rep Phys Sci*, 2022, **3**, 101146.

11 J. Y. Oh, J. H. Lee, S. W. Han, S. S. Chae, E. J. Bae, Y. H. Kang, W. J. Choi, S. Y. Cho, J.-O. Lee, H. K. Baik, and T. I. Lee, *Energy Environ. Sci.*, 2016, **9**, 1696–1705.

12 G. Joshi, D. Mitchell, J. Ruedin, K. Hoover, R. Guzman, M. McAleer, L. Wood and S. Savoy, *J. Mater. Chem. C*, 2019, **7**, 479–483.

13 Q. Zhang, J. Liao, Y. Tang, M. Gu, C. Ming, P. Qiu, S. Bai, X. Shi, C. Uher and L. Chen, *Energy Environ. Sci.*, 2017, **10**, 956–963.

14 L. Yin, C. Chen, F. Zhang, X. Li, F. Bai, Z. Zhang, X. Wang, J. Mao, F. Cao, X. Chen, J. Sui, X. Liu and Q. Zhang, *Acta Mater.*, 2020, **198**, 25–34.

15 L. Yin, F. Yang, X. Bao, W. Xue, Z. Du, X. Wang, J. Cheng, H. Ji, J. Sui, X. Liu, Y. Wang, F. Cao, J. Mao, M. Li, Z. Ren and Q. Zhang, *Nat. Energy*, 2023, **8**, 665–674.

16 A. Singh, S. Bhattacharya, C. Thinaharan, D. K. Aswal, S. K. Gupta, J. V. Yakhmi and K. Bhanumurthy, *J. Phys. D: Appl. Phys.*, 2008, **42**, 015502.

17 P. Qiu, T. Mao, Z. Huang, X. Xia, J. Liao, M. T. Agne, M. Gu, Q. Zhang, D. Ren, S. Bai, X. Shi, G. J. Snyder and L. Chen, *Joule*, 2019, **3**, 1538–1548.

18 L. Xie, C. Ming, Q. Song, C. Wang, J. Liao, L. Wang, C. Zhu, F. Xu, Y.-Y. Sun, S. Bai and L. Chen, *Sci. Adv.*, 2023, **9**, eadg7919.

19 Y. Lu, Y. Qiu, K. Cai, Y. Ding, M. Wang, C. Jiang, Q. Yao, C. Huang, L. Chen, and J. He, *Energy Environ. Sci.*, 2020, **13**, 1240–1249.

20 Y. Ding, Y. Qiu, K. Cai, Q. Yao, S. Chen, L. Chen and J. He, *Nat Commun*, 2019, **10**, 841.

21 D. Palaporn, W. Mongkolthanaruk, K. Faungnawakij, K. Kurosaki, and S. Pinitsoontorn, *ACS Appl. Energy Mater.*, 2022, **5**, 3489–3501.

22 D.-W. Ao, W.-D. Liu, Z.-H. Zheng, X.-L. Shi, M. Wei, Y.-M. Zhong, M. Li, G.-X. Liang, P. Fan, and Z.-G. Chen, *Adv. Energy Mater.*, 2022, **12**, 2202731.

23 T. Varghese, C. Dun, N. Kempf, M. Saeidi-Javash, C. Karthik, J. Richardson, C. Hollar, D. Estrada, and Y. Zhang, *Advanced Functional Materials*, 2020, **30**, 1905796.

24 X. Zhang, Y. Hou, Y. Yang, Z. Wang, X. Liang, Q. He, Y. Xu, X. Sun, H. Ma, J.

Liang, Y. Liu, W. Wu, H. Yu, H. Guo and R. Xiong, *Advanced Materials*, 2023, **35**, 2207723.

25 T. Shi, M. Chen, C. Zhang, Z. Mao, J. Liang, Z. Liu, J. Zhang, Q. Zhang, L. Pan, Y. Wang, C. Wan and P. Zong, *Appl. Surf. Sci.*, 2022, **610**, 155479.

26 L. Wang, Z. Zhang, L. Geng, T. Yuan, Y. Liu, J. Guo, L. Fang, J. Qiu, and S. Wang, *Energy Environ. Sci.*, 2018, **11**, 1307–1317.

27 P. Yu, R. Wu, C. Liu, J. Lan, Y. H. Lin and X. Yang, *Sustain. Energ. Fuels*, 2023, **7**, 172–180.

28 X. Liu, X.-L. Shi, L. Zhang, W.-D. Liu, Y. Yang and Z.-G. Chen, *Journal of Materials Science & Technology*, 2023, **132**, 81–89.

29 A. Kumari, A. Ghosh, B. R. Mehta and A. Sinha, *ACS Sustain. Chem. Eng.*, 2023, **11**, 4226–4236.

30 X. Li, Z. He, Z. Liu, Y. Chen, Z. Zhou, G. Chen, W. Qi, D. Rauber, C. W. M. Kay and P. Zhang, *Chem. Eng. J.*, 2022, **454**, 140047.

31 Y. Liu, S. Hou, X. Wang, L. Yin, Z. Wu, X. Wang, J. Mao, J. Sui, X. Liu, Q. Zhang, Z. Liu, and F. Cao, *Small*, 2022, **18**, e2106875.

32 F. Suarez, D. P. Parekh, C. Ladd, D. Vashaee, M. D. Dickey, and M. C. Öztürk, *Appl. Energy*, 2017, **202**, 736–745.

33 S. Khan, J. Kim, K. Roh, G. Park, and W. Kim, *Nano Energy*, 2021, **87**, 106180.

34 V. P. Ramesh, Y. Sargolzaeiaval, T. Neumann, V. Misra, D. Vashaee, M. D. Dickey, and M. C. Ozturk, *npj Flex Electron*, 2021, **5**, 1–12.

35 Y. Sargolzaeiaval, V. P. Ramesh, T. V. Neumann, V. Misra, D. Vashaee, M. D. Dickey, and M. C. Öztürk, *Appl. Energy*, 2020, **262**, 114370.

36 K. Hu, D. Yang, Y. Hui, H. Zhang, R. Song, Y. Liu, J. Wang, P. Wen, D. He, X. Liu, Y. Yan and X. Tang, *J. Mater. Chem. A*, 2022, **10**, 24985–24994.

37 T. N. Huu, T. N. Van, and O. Takahito, *Appl. Energy*, 2018, **210**, 467–476.

38 T. Nishino and T. Suzuki, *J. Micromech. Microeng.*, 2017, **27**, 035011.